Research Article

An *In Vitro* Study for the Detection of Breast Cancer by Computed Tomography Using Targeted Gold Nanoparticles

Mariam Mubarak-Gabrian MD, MS[1], **Ana Maria Zaske** PhD[2], **Patrick Kee** MD, PhD[2] and **Delia Danila** PhD[2]*

[1]Department of Surgical Oncology, University Medical Center Groningen, MWF-complex A. Deusinglaan 1, Groningen, The Netherlands

[2]Department of Internal Medicine, Division of Cardiology, The University of Texas Health Science Center at Houston, 1881 East Road, 3SCR6.4609, Houston, TX 77054-6011, USA

Corresponding author: Delia Danila, Department of Internal Medicine, Division of Cardiology, The University of Texas Health Science Center at Houston, 1881 East Road, Houston, TX, USA; **Tel:** 7134866531

Abstract

Breast cancer is the second most commonly diagnosed type of cancer worldwide and one of the leading causes of death in women in developed countries, second only to lung cancer. Standard clinical imaging techniques such as mammography, ultrasound and MRI can readily identify anatomical patterns, tumor location and size, but they cannot distinguish between benign and malignant lesions and are not able to detect metastases smaller than 0.5 cm. We have developed a targeted gold nanoparticle (AuNP) for the CT detection of breast cancer. To enable homing to breast cancer, AuNPs are coated with 2-Deoxy-D-Glucose that facilitates their binding to the Gluocose transporter (Glut-1), a cellular transmembrane receptor linked to the progression of breast cancer. Breast cancer cells MDA-MB-231, macrophages RAW 264.7 and fibroblasts MC 3T3.E1 were scanned using a pre-clinical CT scanner after incubation with AuNPs to analyze for AuNPs uptake. Breast cancer cells showed the most intense signal for 2-DG-AuNPs (916 HU), with almost no signal registered for the bare AuNPs (22 HU) or for the control sample (19 HU). In conclusion, 2-DG-AuNPs are a feasable targeting contrast agents for breast cancer detection, ensuring high contrast enhancement and low toxicity.

Keywords: Gold nanoparticles, Computed tomography, Breast cancer detection, Contrast agents, Glut-1

Introduction

Breast cancer is the second most commonly diagnosed type of cancer worldwide and one of the leading causes of death in women in developed countries, second only to lung cancer [1,2]. Although the overall 5-year survival rate in patients with breast cancer has improved over the past decades, the disease is still a serious public health threat [3,4]. More than 3.5 million women in the United States are living with a history of breast cancer and in 2014 approximately 41,213 deaths caused by this type of cancer were registered [1,2,5].

Despite the undeniable concern posed by this disease, recent advancements in screening and treatment techniques, such as surgery, radiotherapy and adjuvant systemic therapy (endocrine therapy, chemotherapy with anthracyclines and taxanes) have brought little improvement to the life expectancy and quality of life of breast cancer patients [5]. The golden standard for breast cancer imaging is mammography [6]. Early detection and diagnosis strongly correlate with a better outcome and higher survival rates and there is evidence that mammography screening could reduce breast cancer mortality rates in several countries [6,7]. However, in women with dense breasts, the sensitivity of mammography is only 62.9% and the specificity is 89.1%, as opposed to 87% sensitivity and 96.9% specificity in women with fatty breasts. Younger women are more likely to have dense

breast tissue and cancer lesions are therefore harder to diagnose with conventional mammography in this patient group [6-8]. Moreover, mammography has a sensitivity of only 55-68% for the diagnosis of locally recurrent breast cancer. This is particularly due to the post-operative benign changes that appear after Breast Conserving Surgery (BCS), such as edema, calcifications, asymmetry and skin thickening [8,9]. Another disadvantage would be the discomfort caused by the compression of the breasts and the exposure to high doses of ionized radiation [8].

Standard clinical imaging techniques such as mammography, ultrasound and MRI are classified as structural imaging modalities because although they can readily identify anatomical patterns and tumor location and size, they cannot distinguish between benign and malignant lesions and are not able to detect metastases smaller than 0.5 cm [10]. Due to these limitations, a new field of imaging has been raising interest in recent years: nanoimaging.

Nanoparticles have unique physiological, optical and magnetic characteristics which bring new possibilities to the field of imaging [11,12]. Their size usually ranges between 1-100 nm and they can have different properties depending on shape, size and surface chemistry [10,13,14]. They can be used for imaging specific receptors, vascular abnormalities and even innate immune responses [13].

Mariam Mubarak-Gabrian, Ana Maria Zaske, Patrick Kee and Delia Danila (2020) An *In Vitro* Study for the Detection of Breast Cancer by Computed Tomography Using Targeted Gold Nanoparticles.

Gold nanoparticles (AuNPs) are attractive nanoparticles to study as Computed Tomography (CT) contrast agents [14-16]. Computed Tomography is one of the most common imaging modalities in hospitals as a diagnostic tool, having the advantages of providing superior tissue penetration and spatial resolution [6,17,18]. CT works by visualizing differences between tissue densities, which results in clear anatomical images. However, in order to see the differences between diseased and normal tissues, specific contrast agents need to be used. Radiopaque X-ray contrast agents are usually injected intravenously and exhibit non-specific penetration and binding, as well as rapid renal excretion [19]. These limitations have determined a surge in the research of targeting agents and cellular imaging, using metal-based agents instead of the traditional iodinated ones, such as Omnipaque or Visipaque [17,18,20].

Gold has proven to be an attractive alternative to conventional contrast agents, having a higher atomic number and a higher absorption coefficient compared to iodine. Due to these properties, gold nanoparticles offer a 3-fold increase in contrast per unit weight compared to iodine-based contrast agents [18,19,21]. Moreover, imaging gold nanoparticles at 80-100 kV provides lower soft tissue absorption, as well as allowing the reduction of bone tissue interference [19]. Gold nanoparticles can be prepared in various sizes and can be selected to facilitate specific extravasation through angiogenic endothelium such as those present in the leaking vasculature of cancer cells. Safety is an obvious consideration with any contrast agent. There is extensive experience with the use of gold in the treatment of various inflammatory and infective conditions in humans such as rheumatoid arthritis.

Bare gold nanoparticles exhbit rapid renal clearance. The rapid clearance and aggregation of AuNPs can be prevented by using a coating agent such as Polyethylene Glycol (PEG) [18,19,22,23]. The coating can be done using a short-strand PEG derivative, such as PEG-SH and/or a longer one such as OPSS-PEG-SVA (orthopyridyldisulfide-polyethyleneglycol-N-hydroxysuccinimide). OPSS-PEG-SVA is being used for the covalent couple of a highly specific ligand, resulting in a targeting agent specific for one cellular group.

We have developed a biocompatible targeted radiocontrast agent based on goldnanoparticles (AuNPs) which has the advantages of offering 3-fold greater contrast per unit weight than iodine-based x-ray contrast agents. Glucose transporter (Glut) is a cellular transmembrane receptor linked to the progression of various types of cancer. It had been previously demonstrated that MDA-MB-231 and MCF-7 breast cancer cells are characterized by over-expression of Glut-1. It is also known that 2-deoxy-D-glucose (2-DG) are specific ligands for Glut-1 [24,25]. Our imaging platform consists of 2-deoxy-D-glucose covalently coupled to spherical gold nanoparticles to target Glut-1 over-expressed by breast cancer cells.

Material and Methods

Materials

Sodium citrate, gold chloride and Picrosirius Red stain (Direct Red 80, Picric acid solution and Hematoxylin Solution A according to Weigert) were purchased from Sigma-Aldrich (St. Louis, MO, USA). OPSS-PEG-SVA was purchased from Laysan Bio (Arab, AL, USA). PES membranes (3000 MWCO) were purchased from Fisher Scientific. Silver enhancement staining kit was purchased from Structure Probe, Inc. (West Chester, PA, USA). DMEM, Fibroblast Basal Media and Fibroblast Serum-Free Growth kit were purchased from ATCC (Manassas, VA, USA), Primary anti-Glut1 antibody was purchased from Fisher Scientific, Alexa Fluor 288 goat anti-rabbit IgG (H+L) was purchased from AbCam (Cambridge, MA, USA), Vectashield mounting medium with DAPI was purchased from Vector Laboratories Inc. (Burlingame, CA, USA), Phalloidin was purchased from Invitrogen (Carlsbad, CA, USA), MTT assay kit was purchased from Roche Applied Science (Indianapolis, IN, USA), 2-Deoxy-D-Glucose was purchased from VWR, D (+)-Glucosamine hydrochloride was purchased from Fisher Scientific. Highest grade V1 mica discs 12 mm were purchased from Ted Pella, Inc., (Redding, CA, USA).

Gold Nanoparticle Synthesis

AuNPs were prepared by a method involving the reduction of chloroauric acid with a sodium citrate solution. Nanopure water (500 ml) was filtered through 0.22 μm filter and boiled in a 1 L conical flask. 5 ml of Gold Chloride (10%) was added to the boiling water followed by 4 ml of 1% sodium citrate solution. The solution was boiled for about an hour or until 200 ml of solution was left. The solution has a burgundy color. Next, the AuNPs were pegylated with polyethylene glycol derivatives in order to avoid aggregation. The AuNPs were incubated for 1 hour with a 100:1 molar ratio of PEG-SH to prevent aggregation and with 50:1 OPSS-PEG-SVA for the covalent coupling of the 2-DG. After pegylation, the AuNPs were further concentrated by centrifugation at 3270 rpm for 60 min. The AuNPs collected were further concentrated using PES membrane concentrators (MWCO 10,000) to a final concentration of ~40 mg Au/ml. The AuNPs were characterized in terms of size and polydispersity by UV Spectrophotometry and Dynamic Light Scattering (Malvern Nano-ZS Zetasizer, Malvern Instruments Ltd., a Spectris Company; Worcestershire, UK). The particles were also analyzed by Atomic Force Microscopy.

2-Deoxy-D-Glucose-AuNPs Synthesis

A solution of 2-deoxy-D-glucose (2-DG) (4 mg of 2-DG in 2 mL of nanopure water) was added to 2.2 mL of AuNPs solution (6 nM) and left to stir overnight at room temperature. The unbound 2-DG was removed by centrifugation through PES membrane tubes at 3270 rpm, for 1 hour. The 2-DG-AuNPs were reconstituted with 1 mL of nanopure water.

Assessment of Glut-1 Expression in Cells

The cells were grown overnight on 8-chamber slides. They were fixed with 300 μl of 4% formalin for 10 minutes and then incubated with 500 μl of 1% BSA (10% normal goat serum, 0.3M glycine) in 0.1% PBS-Tween for 1 hour to permeabilize the cells and block non-specific protein-protein interactions. The cells were then incubated with 300 μl of antibody (ab652, 1:1000 dilution) overnight at 4ºC. Next, the cells were washed thouroughly with PBS followed by incubation with the secondary antibody, Alexa Fluor® 288 goat anti-rabbit IgG (H+L),

used at a 1:1000 dilution for 1 hour at room temperature. The cells were washed with PBS and the slides mounted with DAPI-containing mounting media. Phalloidin was used for staining actin filaments. Fluorescence microscopy was used to determine the Glut-1 expression in cells.

Internalization of AuNPs in Cells

The cells were grown overnight on 8-chamber slides. 50 μl of AuNPs solution was added directly into the media and the cells were incubated for 2, 4 and 24 hours at 37°C and 5% CO2. The cells were then washed three times with warmed PBS and fixated with 300 μl of 4% formaldehyde for 20 minutes at room temperature. The cells were washed three times with PBS and then incubated with 100 μl of Hematoxylin for 15 minutes to stain the nuclei. After the cells were washed again, they were stained for Au with 100 μl of silver staining for 12 minutes. The slides were then washed and dried followed by mounting. Light microscopy was performed to determine the distribution of AuNPs retention in the cells.

Atomic Force Microscopy (AFM) Analysis

Gold nanoparticles were characterized using AFM. Freshly cleaved mica surface was treated with 10 μl of APTES (1 μM in miliQ-water) for 5 min and rinsed with 2 ml of miliQ-water (AP-mica). A drop of 10 μl of AuNPs suspension (to a concentration of 200 μg/ml) was incubated for 15 min at room temperature on functionalized mica (AP-mica) and rinsed with 60 μl of miliQ-water. Excess of liquid was absorbed and let it dry to be immediately scanned after preparation.

Atomic Force Microscopy was conducted at the UT Health - AFM Core Facility using a BioScope II™ Controller (Bruker Corporation; Santa Barbara, CA). This system is integrated to a Nikon TE2000-E inverted optical microscope (Nikon Instruments Inc.; Lewisville, TX). The image acquisition was performed with the Research NanoScope software version 7.30 and analyzed with the NanoScope Analysis software version 1.40 (copyright 2013 Bruker Corporation). High resolution images of AuNPs were obtained using RTESP cantilevers (*fo*=237-289 kHz, *k*=20-80 N/m, Bruker Corporation, Santa Barbara, CA). AuNPs size was determined using tapping mode operated in air to a scan rate of 0.5-0.6 Hz. Particle analysis was performed in 2 and 3 μm^2 scans.

Computed Tomography Scans

One milliliter of cell suspension (10^5 cells/mL) was mixed with 1 mL of AuNPs (targeted or non-targeted) and allowed to interact for 4 hours at 37°C. PBS was used as control. Then, the solutions were centrifuged 3 times at 1000 rpm for 5 minutes, to wash out unbound AuNPs. After each centrifugation step the mixture was resuspended in PBS solution (1 mL total volume).

The cell suspensions were then analyzed with computed tomography. CT imaging was performed with a GE Ultra flat panel CT scanner (General Electric, Milwaukee, WI) with the following acquisition settings: 80kVp, 22 mA with 16 s rotation/exposure. Simple back projections were obtained for the 0.154 μm image reconstruction and exported as DICOM images. Image analysis was performed using the OsiriX software.

Results

The gold nanoparticles were synthesized by citrate reduction, using the Turkevich method. All the AuNPs preparations used in this study were analyzed using UV spectrometry, DLS, and atomic force microscopy (AFM). For all the samples, the UV absorbance peaked at 540 nm that corresponds to 60 nm particles. The AFM analysis showed a uniform preparation of AuNPs of 40-50 nm, at 2.0 μm scan zise (Figure 1). The DLS data showed a diameter of 46 nm with a polydispersity index (PDI) value of 0.451 for the bare AuNP samples. 2-DG-AuNPs had a diameter of 43 nm with a PDI value of 0.374.

Colloidal gold has been found to be unstable in a saline environment. The AuNPs were stabilized using a functionalized long chain PEG with a molecular weight of 5 kDa (OPSS-PEG-SVA) to prevent the formation of aggregates and rapid clearance in vivo. Moreover, OPSS-PEG-SVA had functional groups available for covalent bonding which allowed the conjugation via strong gold-thiolate bonds of a specific ligand (a D-glucose analogue).

Glut-1 expression was assessed using immunocytochemistry by staining Glut-1 receptors with green Alexa Fluor® 288 goat anti-rabbit IgG (H+L). Breast cancer cells MDA-MB-231 (image B, Figure 2) and macrophage cells RAW 264.7 (image A, Figure 2) showed Glut-1 receptor expression when compared to fibroblast control cells MC 3T3.E1 (image C, Figure 2). Fibroblasts did not display any Glut-1 expression.

Gold nanoparticle uptake was analyzed after incubating the cells with targeted or non-targeted AuNPs solution for four hours. The gold nanoparticles were stained with silver and appear as small black particles on the light microscopy images (Figure 3).
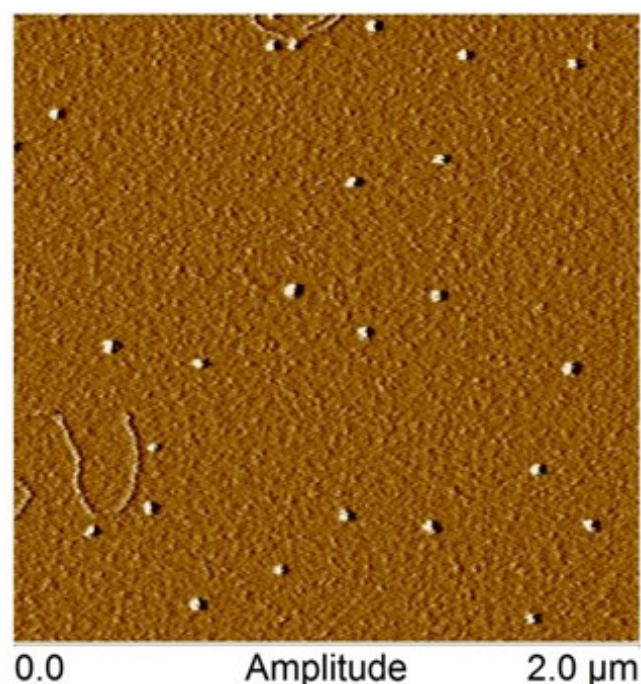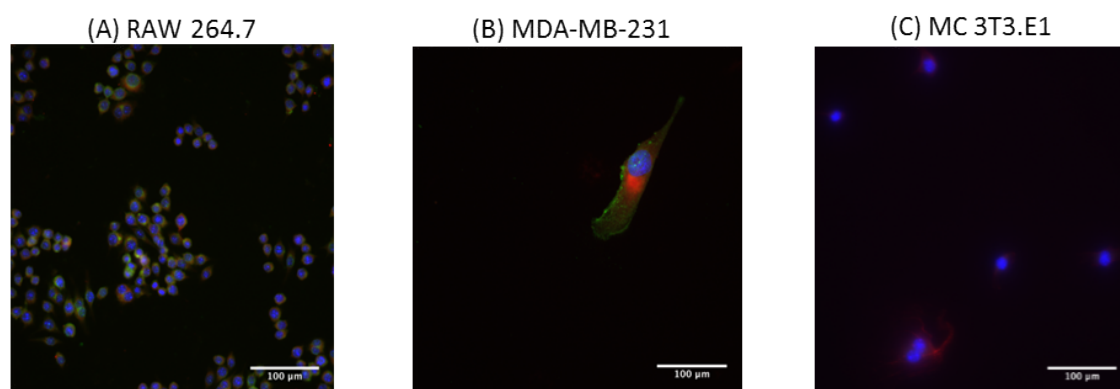

Figure 1: AFM amplitude image of gold nanoparticles scaned at 2 μm (X-Y) in tapping mode in air.

Figure 2: Fluorescence microscopy images of Glut-1 expression in RAW 264.7 macropages (image A), MDA-MB-231 breast cancer cells (image B) and MC 3T3.E1 fibroblasts (image C); scale bar represents 100 μm. Glut-1 expression is observed in RAW 264.7 and MDA-MB-231 breast cancer cells, but not in MC 3T3.E1 fibroblasts (green color).
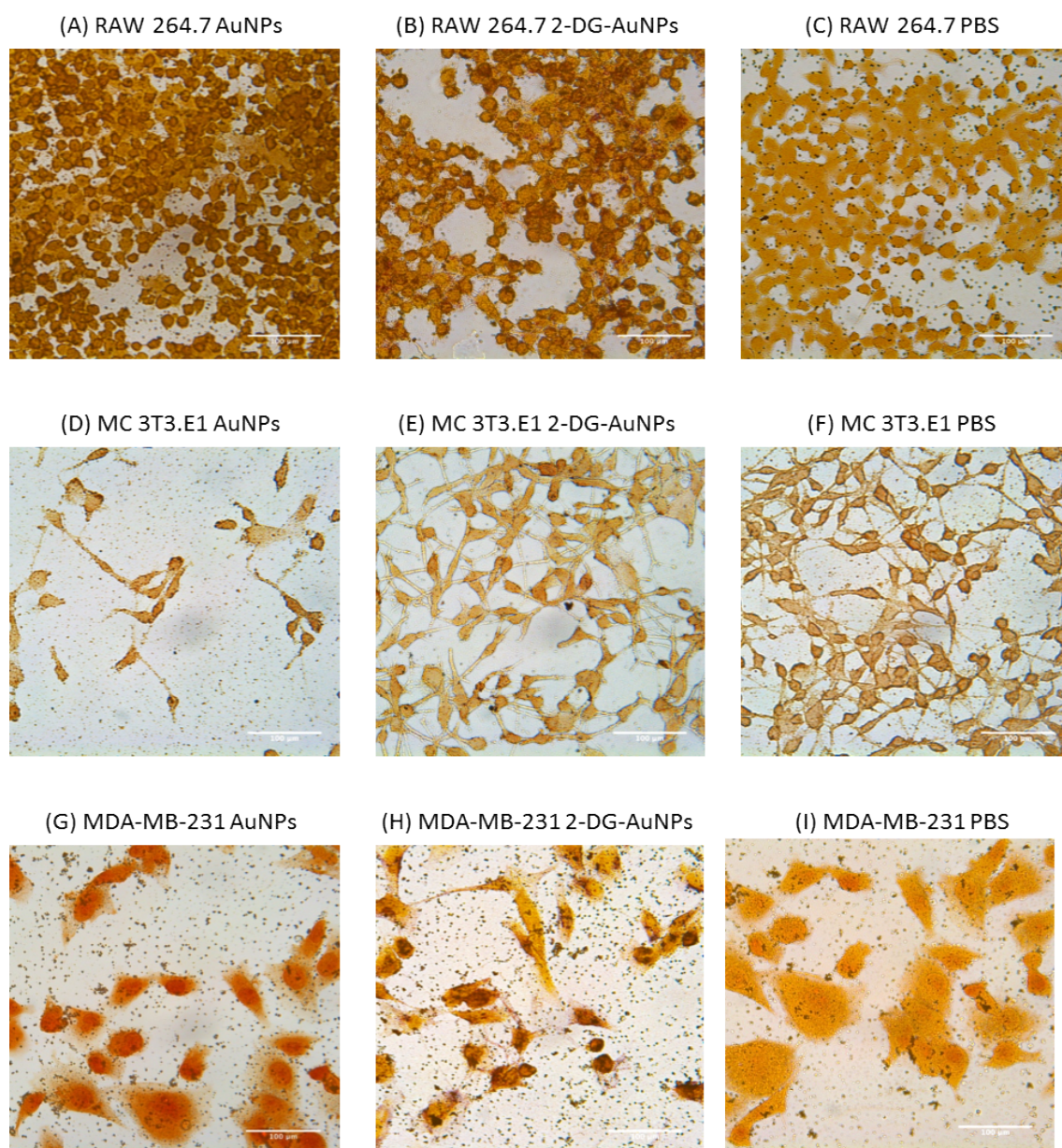
Figure 3: Light microscopy images of gold nanoparticle internalization in RAW 264.7 macrophage (A-C), MC 3T3.E1 fibroblast (D-F), and MDA-MB-231 breast cancer cells (G-I) cell lines; scale bar is equal to 100 μm. 2-DG-AuNPs are taken-up by MDA-MB-231 (C) and RAW 264.7 cells (F). Very little non-specific uptake of bare AuNPs is observed in MDA-MB-231 (B) and RAW 264.7 cells (E). No uptake of bare AuNPs (H) or 2-DG-AuNPs (I) is observed in MC 3T3.E1.

Mariam Mubarak-Gabrian, Ana Maria Zaske, Patrick Kee and Delia Danila (2020) An *In Vitro* Study for the Detection of Breast Cancer by Computed Tomography Using Targeted Gold Nanoparticles.

Both breast cancer cells MDA-MB-231 and macrophage cells RAW 264.7 displayed AuNPs internalization as compared to fibroblast cells MC 3T3.E1 (Figure 3). Macrophages showed the most uptake of the targeted AuNPs which can be noted because of the presence of darker aggregates inside the cells (image F, Figure 3). Fibroblasts showed no difference in gold nanoparticle uptake between the AuNPs, 2-DG-AuNPs, and control (images G-I, Figure 3).

Breast cancer cells MDA-MB-231, macrophages RAW 264.7 and fibroblasts MC 3T3.E1 were scanned using a pre-clinical CT. The cells were incubated with targeted or non-targeted AuNPs for 4 hours followed by extensive washing. Breast cancer cells showed the most intense signal for 2-DG-AuNPs at 916 HU (Image C, Figure 4) with almost no signal registered for the bare AuNPs at 22 HU (Image B, Figure 4) or the control sample at 19 HU (Image A, Figure 4). No signal was visible on the scan in the control and bare AuNPs sample (Figure 4).

For the RAW 264.7 macrophages, the 2-DG-AuNPs sample also displayed the highest radiointensity at 767 HU (Image F, Figure 4), followed by bare AuNPs at 140 HU (Image E, Figure 4). No signal was visible on the scan for the control (image D, Figure 4). Control samples registered 20 HU for fibroblast cells. The MC 3T3.E1 registered baseline values for all the samples analyzed (Images G-I, Figure 4).

Discussion

Medical imaging techniques can be divided into structural and functional imaging. Recently, functional imaging has been gaining interest over more conventional anatomical imaging. This came as a response to the need for earlier detection of malignant tissues and metastases, which were not visible through structural scans. This study proposed a novel approach to functional imaging using gold nanoparticles to target a ligand specific to mesenchymal breast cancer cells and macrophages. The imaging platform consisted of 2-deoxy-D-glucose covalently coupled to spherical gold nanoparticles to
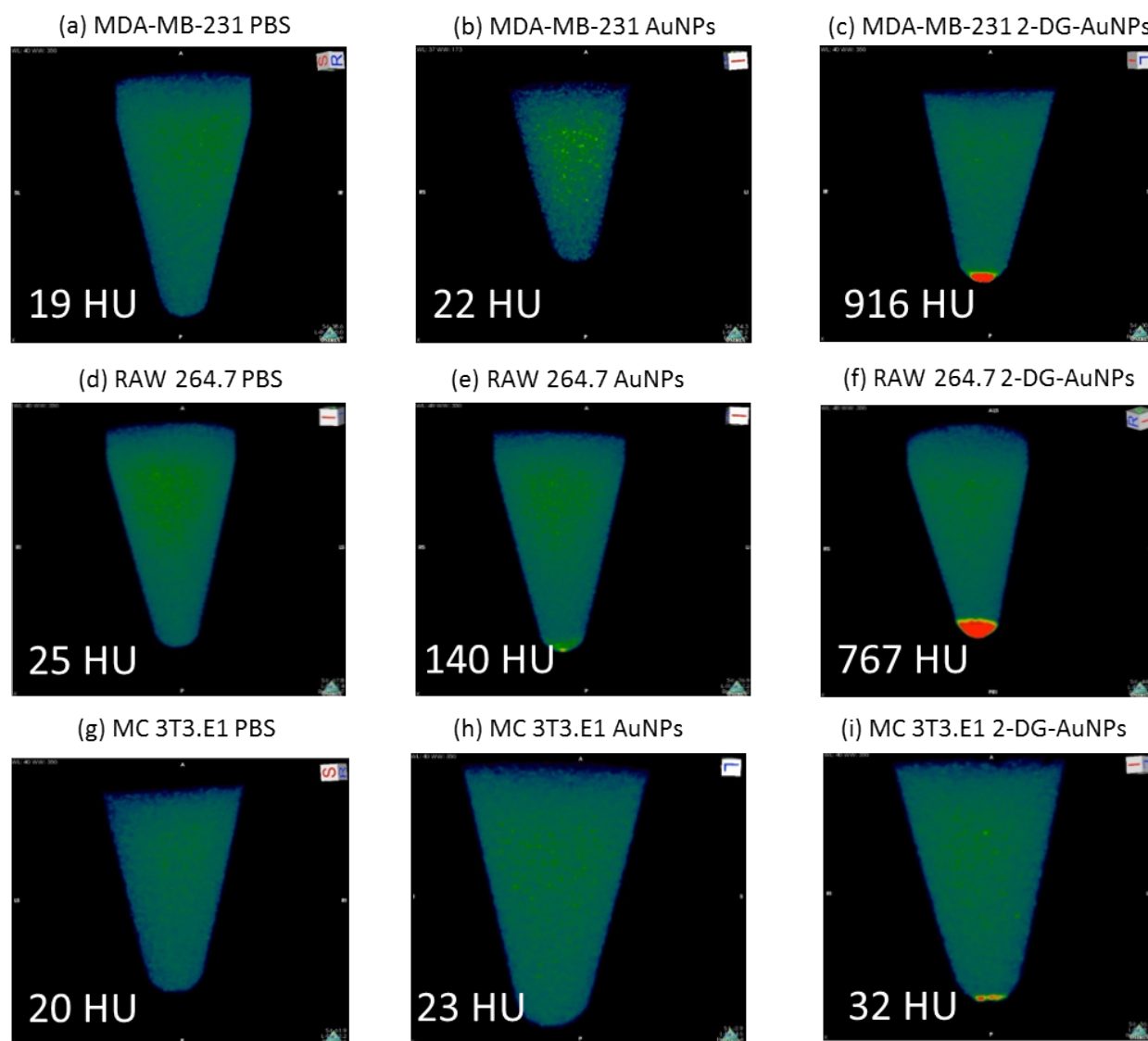
Figure 4: *In vitro* CT imaging of AuNPs internalization in MDA-MB-231 (A-C), RAW 264.7 (D-F), and MC 3T3.E1 (G-I) cells. Samples that display a higher uptake signal appear red on the CT images. The intensity of the red spots are quantified in Hounsfield Units (HU) included in each image. Approximately 40-fold higher attenuation and 5-fold higher attenuation is observed for the 2-DG-AuNPs as compared to bare AuNPs for the MDA-MB-231 cells and RAW 264.7, respectively.

target Glut-1 over-expression in breast cancer cells. The feasibility of this platform was examined using CT imaging and histological staining.

One of the advantages of the proposed imaging technique is the use of a novel targeting agent (AuNPs) which provides superior X-ray attenuation over conventional iodine-based contrast agents. Moreover, it provides the specific targeting of cancer cells with a ligand against the Glut-1 overexpressed by breast cancer cells and macrophages. CT imaging offers excellent tissue penetration and spatial resolution as well as rapid image acquisition.

Carcinoma cells have been proven to have a higher metabolic rate as well as faster proliferation, which leads to greater demand of glucose. Such metabolic characteristics can be linked to the over-expression of certain glucose transporters, such as Glut-1 or Glut-4, on malignant cell membranes. Glut-1 has been proved to be expressed by almost all cancerous cell types [24,25]. The receptor binds and transports D-glucose within the cell, which is further metabolized into D-glucose-6-phosphate and 1,2-diphosphate [24]. D-glucose analogues can be transported by Glut-1 or Glut-4 receptors, but cannot be fully metabolized, therefore remaining inside the cells for longer periods before excretion. This property allows analogues such as 2-DG to be used as specific ligands for malignant cells. Positron emission tomography (PET) scans with radioactive Fluorodeoxyglucose (FDG) use the glucose pathway described to successfully target cancerous lesions and metastases, which are not always visible through structural imaging techniques. Targeting a metabolic mechanism instead of a cell membrane receptor is one of the most promising developments in cancer research and could eventually lead to better drug delivery systems and overcoming drug-resistance [24,25].

MDA-MB-231 is a breast cancer cell line that is known to overexpress Glucose transporter 1 (Glut-1). These types of cancer cells have a high risk of metastasis and an intermediate response to chemotherapy [25-28]. Previous studies show that RAW 264.7 cells also overexpress Glut-1 transporters and therefore exhibit increased glucose uptake and metabolism [29,30].

We were able to demonstrated Glut-1 expression by Immunocytochemistry (Figure 2) and ELISA (results not shown). Following staining with Glut-1 antibody (green), MDA-MB-231 cells showed the highest Glut-1 expression (most intense green coloration), followed by RAW 264.7. Fibroblasts MC 3T3.E1 were used as a control group and displayed no Glut-1 expression (Figure 2). A pilot study was first conducted to determine the adequate incubation time with gold nanoparticles. Cells were incubated with AuNPs for 2, 4 and 24 hours and the results were analyzed histologically. It was concluded that 2 hours did not allow sufficient gold internalization, while 24 hours allowed too much time for the clearance of the nanoparticles. Therefore the 4-hour time point was used in the following experiments.

The AuNPs internalization was first observed histologically, using a silver staining to stain the nanoparticles. Silver staining gave AuNPs a dark, almost black coloration. Therefore, when comparing MDA-MB-231 and RAW 264.7 slides to MC 3T3.E1, a darker coloration of the Glut-1 expressing cells can be noted due to small dark aggregates

present inside said cells. Moreover, MDA-MB-231 and RAW 264.7 cells which were incubated with PBS confirm these results, displaying a light coloration, with no dark particles visible (Figure 3). When comparing bare AuNPs and functionalized 2-DG-AuNPs, a slight difference could be noted in MDA-MB-231 cells, which displayed higher internalization for functionalized nanoparticles (Figure 3). However, for RAW 264.7 cells, the amount of internalization for bare AuNPs and 2-DG-AuNPs was similar (Figure 3). A reason for this could be the presence of other mechanisms (independent of glucose transporters) for internalization in macrophage cells.

The 2-DG-AuNPs were then tested using a pre-clinical CT. As the cells were washed and centrifuged before scanning, the cells gathered at the bottom of the sample tubes, forming cell pellets. The radiointensity measurements were done in triplicates using values from the bottom of the sample tubes, representative for each cell group. It could be noted that 2-DG-AuNPs displayed the highest radiointensity both when measured with the OsiriX software and visually on the scans for the MDA-MB-231 cells (Images A-C, Figure 4) and RAW 264.7 cells (Images D-F, Figure 4). 2-DG-AuNPs registered values of 916 HU for MDA-MB-231 cells and 767 HU for RAW 264.7 cells. The bare AuNPs registered values of 22 HU for MDA-MB-231 cells and 140 HU for RAW 264.7 cells.The PBS controls showed baseline values of 19 HU and 25 HU, respectively. MC 3T3.E1 cells displayed baseline values 20-32 HU.

The attenuation coefficient for the 2-DG targeted AuNPs was approximately 40-fold higher than that of the bare AuNPs for MDA-MB-231 breast cancer cells and 5-fold higher for RAW 264.7 cells.

Breast cancer cells express a high level of GLUT-1 receptors. By harnassing the increased metabolic demand and uptake, tracers such as the functionalized 2-DG-AuNPs is an attractive option to detect the cancer cells. This study was the first attempt at using gold nanoparticles functionalized with 2-deoxy-D-glucose to trace and image breast cancer and tumor-associated macrophages. Functionalized 2-DG-AuNPs proved to be a valid targeting contrast agent for cell lines MDA-MB-231 and RAW 264.7, exhibiting high radiointensity upon CT imaging. Gold internalization was verified with histological and radiological techniques and the positive results indicate a need for further research into this topic, such as testing the concept in vivo in a mouse model of breabt cancer. The targeting agent developed, 2-DG-AuNPs, promises to be a cheap and safe alternative for other types of functional imaging techniques such as nuclear imaging with radioactive fluorodeoxyglucose (FDG).

Acknowlegement

Mariam Mubarak-Gabrian, Ana Maria Zaske, Patrick Kee and Delia Danila (2020) An *In Vitro* Study for the Detection of Breast Cancer by Computed Tomography Using Targeted Gold Nanoparticles.

References

1. Ferlay J, Soerjomataram I, Dikshit R, Eser S, Mathers C, et al. (2015) Cancer incidence and mortality worldwide: Sources, methods and major patterns in GLOBOCAN. *International Journal of Cancer* 136: 359-386. [crossref]

2. Siegel RL, Miller KD, Jemal A (2016) Cancer statistics. *CA: A Cancer Journal for Clinicians* 66: 7-30.

3. Falagan-Lotsch P, Grzincic EM, Murphy CJ (2017) New Advances in Nanotechnology-Based Diagnosis and Therapeutics for Breast Cancer: An Assessment of Active-Targeting Inorganic Nanoplatforms. *Bioconjug Chem* 28: 135-152. [crossref]

4. Berry DA, Cronin KA, Plevritis SK, Fryback DG, Clarke L, et al. (2005) Effect of Screening and Adjuvant Therapy on Mortality from Breast Cancer. *N Engl J Med* 353: 1784-1792. [crossref]

5. Freddie B, McCarron P, Parkin MD (2004) The changing global patterns of female breast cancer incidence and mortality. *Breast Cancer Research* 6: 229-239. [crossref]

6. Jalalian A, Mashohor S, Mahmud R, Karasfi B, Iqbal Saripan M, et al. (2017) Computer-Assisted Diagnosis System for Breast Cancer in Computed Tomography Laser Mammography (CTLM). *J Digit Imaging* 30: 796-811. [crossref]

7. Carney PA, Miglioretti DL, Yankaskas BC, Kerlikowske K, Rosenberg R, et al. (2003) Individual and combined effects of age, breast density, and hormone replacement therapy use on the accuracy of screening mammography. *Ann Intern Med* 138: 168-175. [crossref]

8. Ponhold L, Bickel H, Pinker K, Helbich T (2012) Mammography screening and follow-up of breast cancer. *Hamdan Medical Journal* 5.

9. Kim SJ, Moon WK, Cho N, Chang JM (2011) The detection of recurrent breast cancer in patients with a history of breast cancer surgery: comparison of clinical breast examination, mammography and ultrasonography. *Acta Radiol* 52: 15-20. [crossref]

10. Popovtzer R, Agrawal A, Kotov NA, Popovtzer A, Balter J, et al. (2008) Targeted gold nanoparticles enable molecular CT imaging of cancer. *Nano Lett* 8: 4593-4596. [crossref]

11. Polo E, Collado M, Pelaz B, Del Pino P (2017) Advances toward More Efficient Targeted Delivery of Nanoparticles in Vivo: Understanding Interactions between Nanoparticles and Cells. *ACS Nano* 11: 2397-2402. [crossref]

12. Zhang Y, Hensel M (2013) Evaluation of nanoparticles as endocytic tracers in cellular microbiology. *Nanoscale* 5: 9296-9309.

13. Langer R, Weissleder R (2015) Nanotechnology. *JAMA* 313: 135-136.

14. Pillai G, Ceballos-Coronel ML (2013) Science and technology of the emerging nanomedicines in cancer therapy: A primer for physicians and pharmacists. *SAGE* 1.

15. Giljohann DA, Seferos DS, Daniel WL, Massich MD, Patel PC, et al. (2010) Gold nanoparticles for biology and medicine. *Angew Chem Int Ed Engl* 49: 3280-3294. [crossref]

16. Hornos Carneiro MF, F Barbosa Jr (2016) Gold nanoparticles: A critical review of therapeutic applications and toxicological aspects. *J Toxicol Environ Health B Crit Rev* 19: 129-148. [crossref]

17. Chhour P, Naha PC, O'Neill SM, Litt HI, Reilly MP, et al. (2016) Labeling monocytes with gold nanoparticles to track their recruitment in atherosclerosis with computed tomography. *Biomaterials* 87: 93-103. [crossref]

18. Danila D, Johnson E, Kee P (2013) CT imaging of myocardial scars with collagen-targeting gold nanoparticles. *Nanomedicine* 9: 1067-1076. [crossref]

19. Leung K (2004) Polyethylene glycol-gold nanoparticles. Molecular Imaging and Contrast Agent Database (MICAD) Bethesda (MD).

20. Reuveni T, Motiei M, Romman Z, Popovtzer A, Popovtzer R (2011) Targeted gold nanoparticles enable molecular CT imaging of cancer: an in vivo study. *Int J Nanomedicine* 6: 2859-2864.

21. Connor EE, Mwamuka J, Gole A, Murphy CJ, Wyatt MD (2005) Gold nanoparticles are taken up by human cells but do not cause acute cytotoxicity. *Small* 1: 325-327. [crossref]

22. Otsuka H, Nagasaki Y, Kataoka K (2003) PEGylated nanoparticles for biological and pharmaceutical applications. *Adv Drug Deliv Rev* 55: 403-419. [crossref]

23. Cai QY, Kim SH, Choi KS, Kim SY, Byun SJ, et al. (2007) Colloidal gold nanoparticles as a blood-pool contrast agent for X-ray computed tomography in mice. *Invest Radiol* 42: 797-806. [crossref]

24. Shan XH, Hu H, Xiong F, Gu N, Geng XD, et al. (2012) Targeting Glut1-overexpressing MDA-MB-231 cells with 2-deoxy-D-g1ucose modified SPIOs. *Eur J Radiol* 81: 95-99.

25. Venturelli L, Nappini S, Bulfoni M, Gianfranceschi G, Dal Zilio S, et al. (2016) Glucose is a key driver for GLUT1-mediated nanoparticles internalization in breast cancer cells. *Sci Rep* 6: 21629. [crossref]

26. Holliday DL, Speirs V (2011) Choosing the right cell line for breast cancer research. *Breast Cancer Res* 13: 215. [crossref]

27. Su S, Liu Q, Chen J, Chen J, Chen F, et al. (2014) A positive feedback loop between mesenchymal-like cancer cells and macrophages is essential to breast cancer metastasis. *Cancer Cell* 25: 605-620. [crossref]

28. Shroff K, Kokkoli E (2012) PEGylated liposomal doxorubicin targeted to alpha5beta1-expressing MDA-MB-231 breast cancer cells. *Langmuir* 28: 4729-4736. [crossref]

29. Green CE, Liu T, Montel V, Hsiao G, Lester RD, et al. (2009) Chemoattractant signaling between tumor cells and macrophages regulates cancer cell migration, metastasis and neovascularization. *PLoS One* 4: 6713. [crossref]

30. Freemerman AJ, Johnson AR, Sacks GN, Milner JJ, Kirk EL, et al. (2014) Metabolic reprogramming of macrophages: glucose transporter 1 (GLUT1)-mediated glucose metabolism drives a proinflammatory phenotype. *J Biol Chem* 289: 7884-7896. [crossref]